**Supporting Information**

# High-performance low-cost n-type Se-doped $Mg_3Sb_2$-based Zintl compounds for thermoelectric application

*Jiawei Zhang,[1] Lirong Song,[1] Aref Mamakhel,[1] Mads Ry Vogel Jørgensen,[1,2] and Bo Brummerstedt Iversen[1*]*

[1] *Center for Materials Crystallography, Department of Chemistry and iNANO, Aarhus University, DK-8000 Aarhus, Denmark*
[2] *MAX IV Laboratory, Lund, Sweden*
**E-mail:* bo@chem.au.dk

## Supplementary Figures

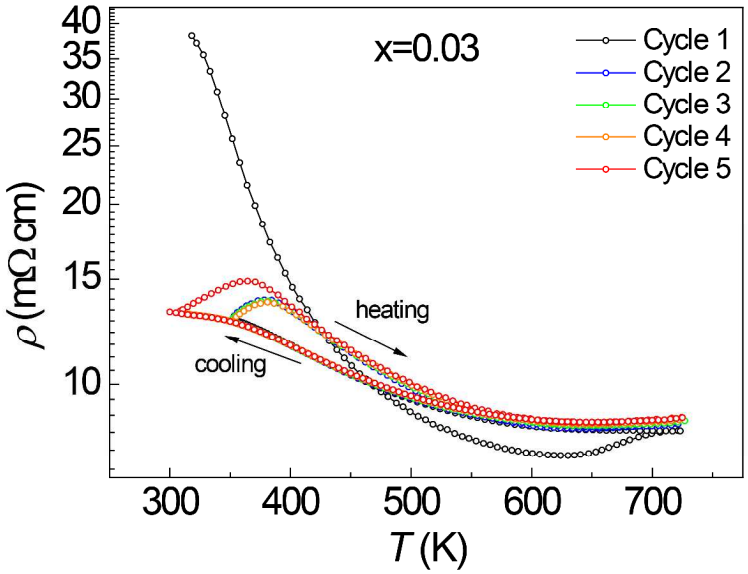


**Figure S1.** Temperature dependence of resistivity with both heating and cooling curves for all 5 cycles in the exemplified n-type $Mg_{3.07}Sb_{1.5}Bi_{0.5-x}Se_x$ ($x$ = 0.03). All other samples typically show the same behavior. The hysteresis loop of the resistivity is stabilized after the first cycle.

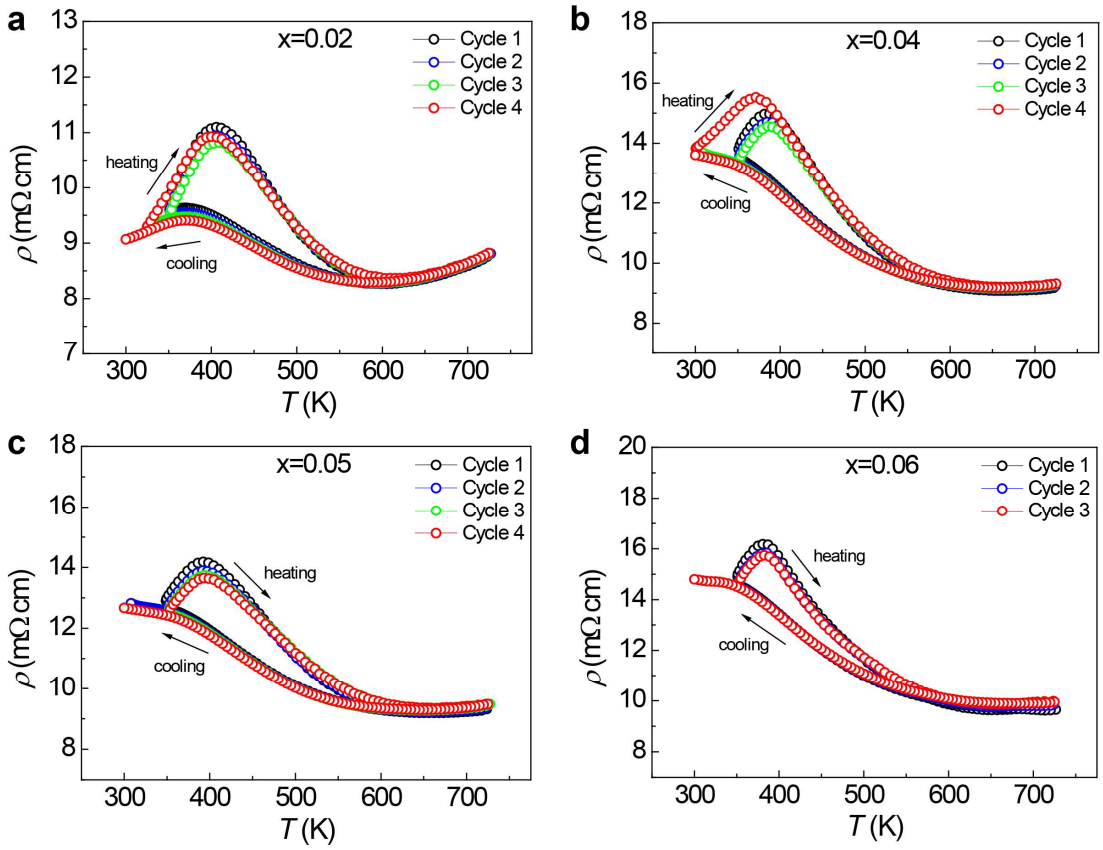


**Figure S2.** Temperature dependence of resistivity with both heating and cooling curves for the stabilized cycles in n-type $Mg_{3.07}Sb_{1.5}Bi_{0.5-x}Se_x$ ($x$ = 0.02, 0.04, 0.05, and 0.06).

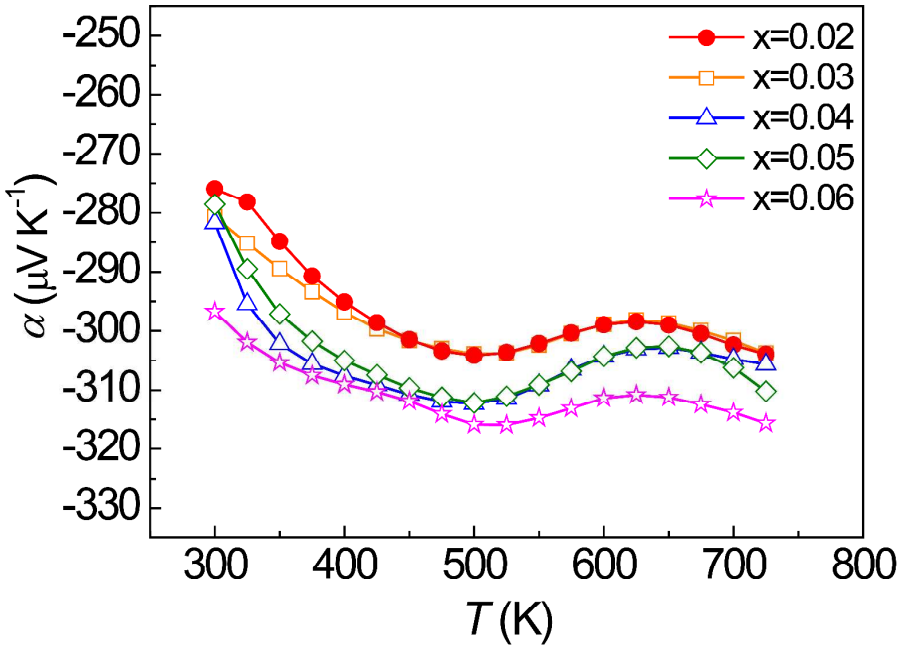


**Figure S3.** Temperature-dependent Seebeck coefficients measured during heating in n-type $Mg_3Sb_{1.5}Bi_{0.5-x}Se_x$ ($x$ = 0.02-0.06).

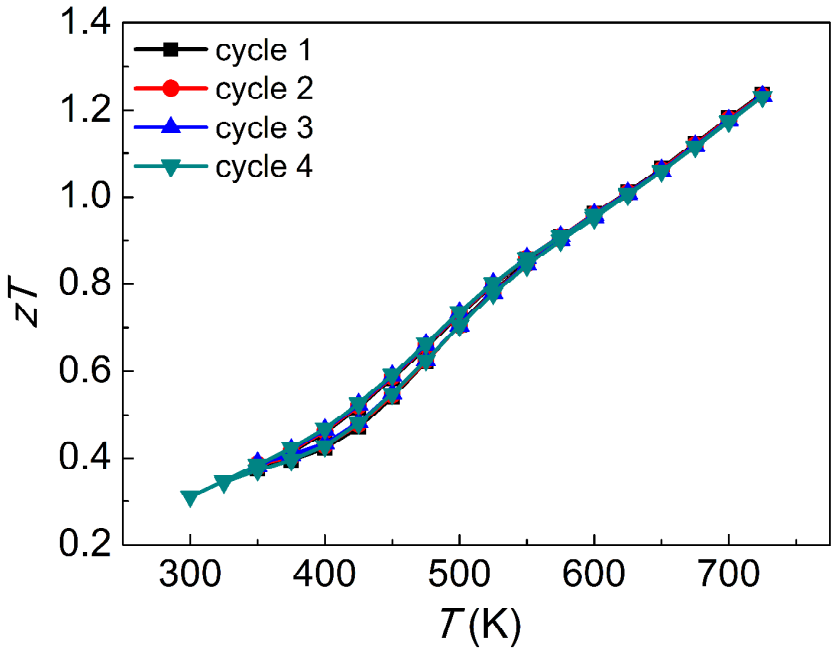


**Figure S4.** Temperature dependence of thermoelectric figure of merit $zT$ in high-performance pellet with $x = 0.02$ calculated from the 4 stabilized cycles of resistivity data.

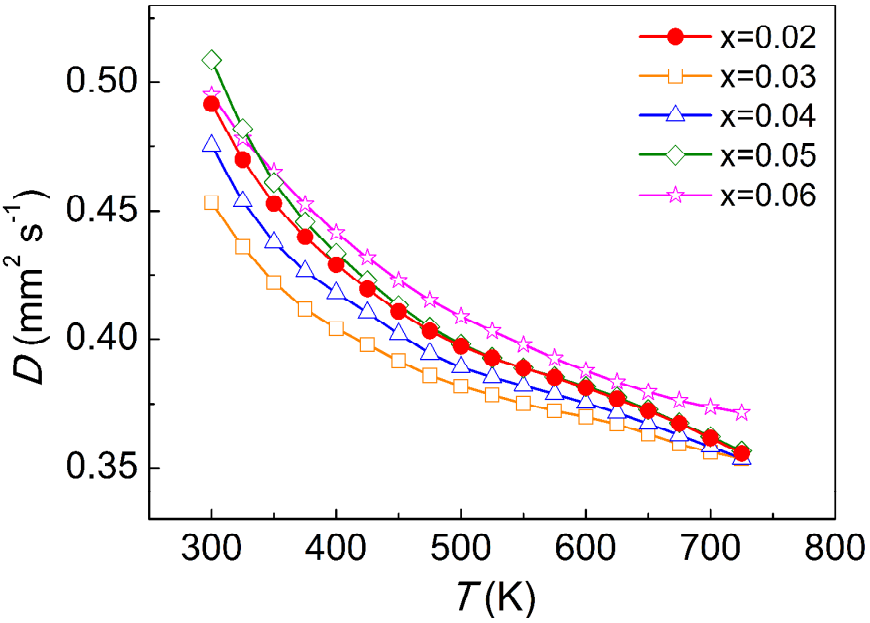


**Figure S5.** Temperature dependence of thermal diffusivity in n-type $Mg_3Sb_{1.5}Bi_{0.5-x}Se_x$ ($x$ = 0.02-0.06).

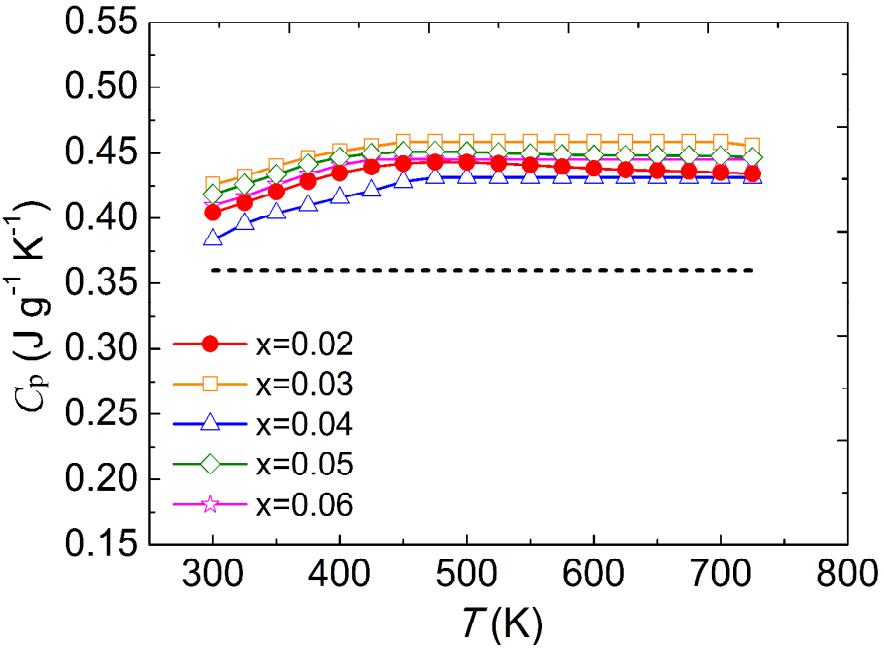


**Figure S6.** The temperature dependence of heat capacity in n-type $Mg_3Sb_{1.5}Bi_{0.5-x}Se_x$ ($x$ = 0.02-0.06). The dashed line represents the Dulong-Petit limit.

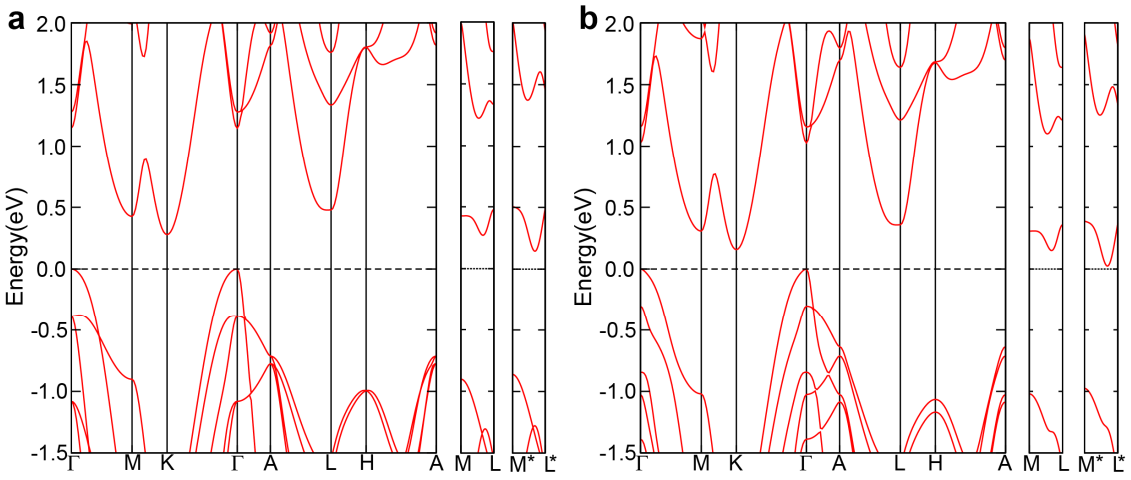


**Figure S7.** Band structures of $Mg_3Sb_2$ calculated by PBE functional[2] (a) without and (b) with spin orbit coupling. The band structures along the $M^*$-$L^*$ are illustrated.

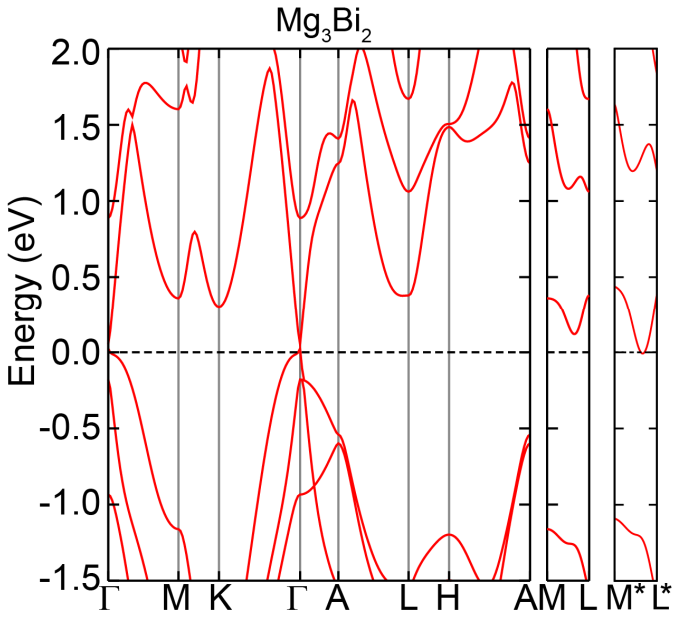


**Figure S8.** Band structure of $Mg_3Bi_2$ calculated by mBJ potential[1] with spin orbit coupling. The band structure along the $M^*$-$L^*$ is illustrated.

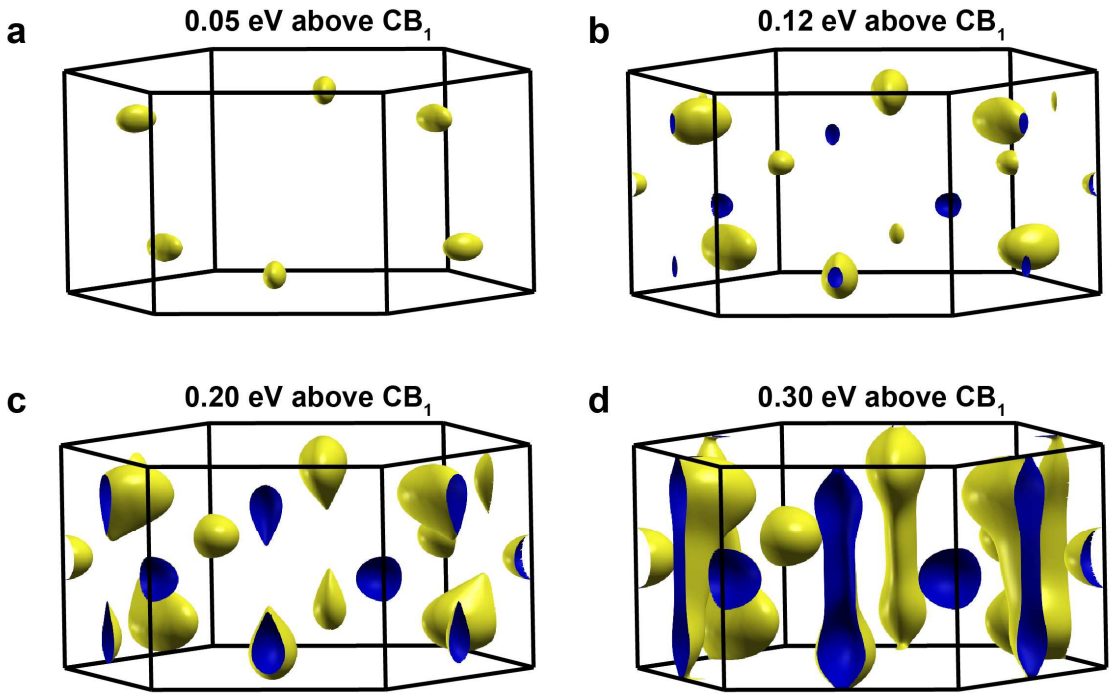


**Figure S9.** Fermi surfaces of n-type $Mg_3Sb_2$ corresponding to energy levels (a) 0.05 eV, (b) 0.12 eV, (c) 0.20 eV, and (d) 0.30 eV above $CB_1$.

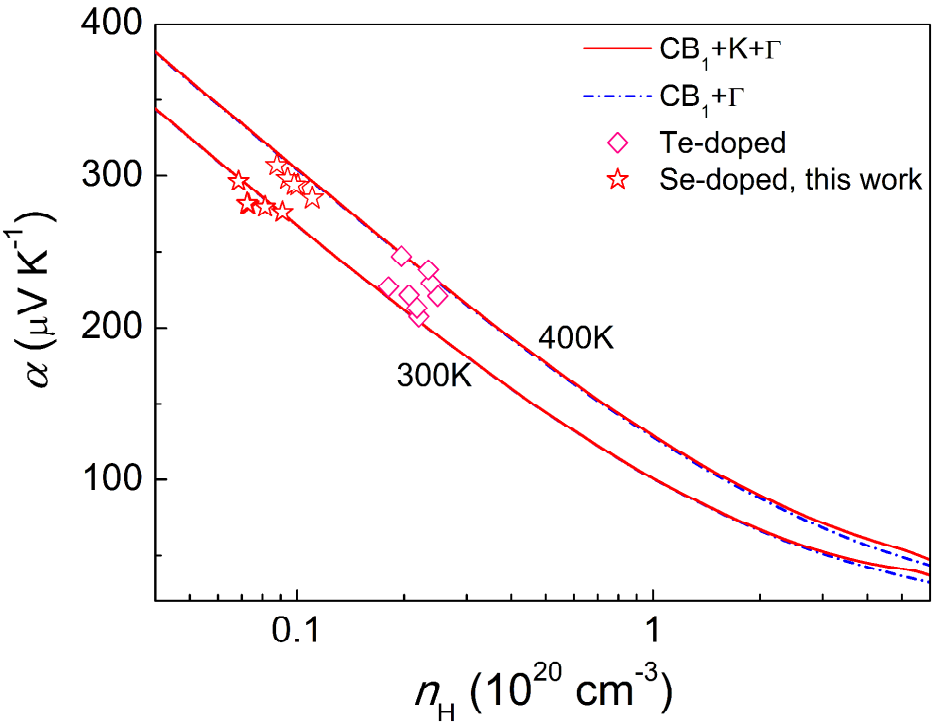


**Figure S10.** The Seebeck coefficient at 300 K (a) and 400 K (b) as a function of Hall carrier concentration. The pink diamond points represent the previously reported n-type Te-doped $Mg_3Sb_{1.5}Bi_{0.5}$.[3] The red star points are Se-doped $Mg_{3.07}Sb_{1.5}Bi_{0.5}$ samples from this work. The red solid lines and the dashed blue lines represent the predictions from a three band model including the $CB_1$, K, and Γ bands ($CB_1$+K+Γ) and a two band model considering the $CB_1$ and Γ bands ($CB_1$+Γ), respectively.

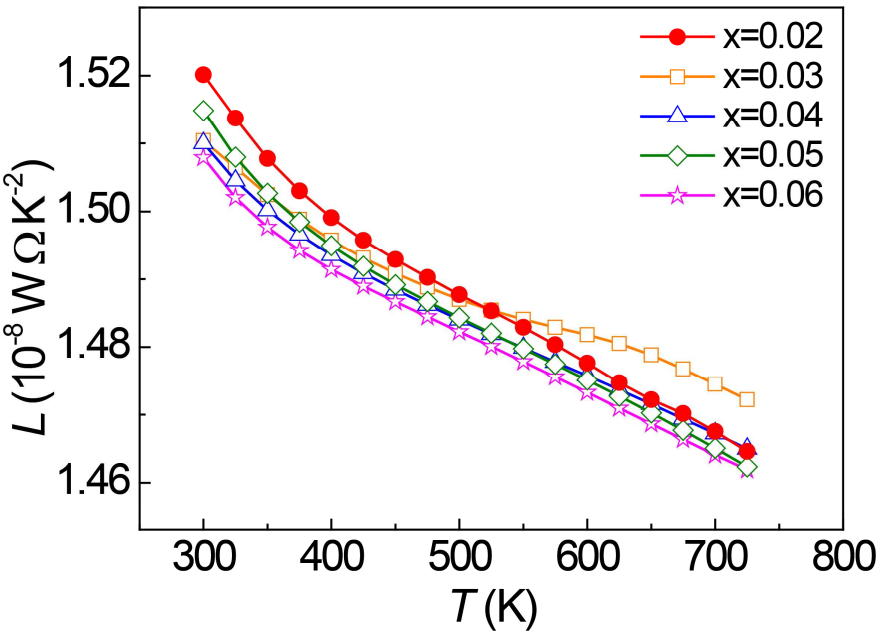


**Figure S11.** The Lorenz number of n-type $Mg_3Sb_{1.5}Bi_{0.5-x}Se_x$ calculated by a three band model as a function of temperature.

## Supplementary Tables

**Table S1.** The sample density of n-type $Mg_3Sb_{1.5}Bi_{0.5-x}Se_x$ ($x$ = 0.02-0.06) measured by Archimedes method.

| Samples | Density (g $cm^{-3}$) | Relative density (%) |
|---|---|---|
| $x$=0.02 | 4.01 | 90.2 |
| $x$=0.03 | 4.03 | 90.5 |
| $x$=0.04 | 4.05 | 91.0 |
| $x$=0.05 | 4.11 | 92.3 |
| $x$=0.06 | 4.07 | 91.5 |

**Table S2.** The location of the accurate conduction band minimum $CB_1$ with a series of denser k-points and different methods (PBE functional[2] or mBJ potential[1]). It is clear that the denser k-points only lead to the negligible effect on the location of $CB_1$, indicating the coordinate of $CB_1$ is well converged.

| k mesh | Number of k points in BZ | Method | Location of $CB_1$ |
|---|---|---|---|
| 36×36×24 | 31104 | PBE/mBJ | (0, 0.417, 0.333) |
| 45×45×24 | 48600 | PBE/mBJ | (0, 0.422, 0.333) |
| 56×56×30 | 94080 | PBE/mBJ | (0, 0.411, 0.333) |

**Table S3.** Physical properties of $Mg_3Sb_{1.5}Bi_{0.5}$ that used for the electronic transport modelling.

| Parameters | $Mg_3Sb_{1.5}Bi_{0.5}$ |
|---|---|
| Band gap (eV) | 0.33 |
| Energy gap (eV) at $CB_1$ point | 1.5 |
| Energy gap (eV) at Γ point | 1.25 |
| Energy difference (eV) between $CB_1$ and K | 0.22 |
| Effective mass ($m_{kx}$, $m_{ky}$, $m_{kz}$) at $CB_1$ | ($0.55m_e$, $0.21m_e$, $0.28m_e$) |
| Effective mass ($m_{kx}$, $m_{ky}$, $m_{kz}$) at K point | ($0.32m_e$, $0.32m_e$, $0.21m_e$) |
| Effective mass ($m_{kx}$, $m_{ky}$, $m_{kz}$) at Γ point | ($1.15m_e$, $1.15m_e$, $0.15m_e$) |
| Valley degeneracy of the conduction band $CB_1$ | 6 |
| Valley degeneracy of the conduction band K | 2 |
| Valley degeneracy of the valence band Γ | 1 |
| DOS effective mass $m^*$ ($m_e$) of the conduction band $CB_1$ | 1.05 |
| DOS effective mass $m^*$ ($m_e$) of the conduction band K | 0.44 |
| DOS effective mass $m^*$ ($m_e$) of the valence band Γ | 0.58 |
| Conductivity effective mass $m_1^*$ ($m_e$) of the conduction band $CB_1$ | 0.30 |
| Conductivity effective mass $m_1^*$ ($m_e$)of the conduction band K | 0.27 |
| Conductivity effective mass $m_1^*$ ($m_e$) of the valence band Γ | 0.36 |
| The average longitudinal elastic constant $C_l$(GPa) | 48.3(ref. 4) |
| Acoustic deformation potential (eV) of the conduction band $CB_1$ | 23.2 |
| Acoustic deformation potential (eV) of the conduction band K | 13.6 |
| Acoustic deformation potential (eV) of the valence band Γ | 27.2 |
| Static dielectric constant $\varepsilon_0$ | 17.4 |
| High-frequency dielectric constant $\varepsilon_\infty$ | 15.7 |
| Alloy scattering potential (eV) | 1.0 |

## Supplementary Notes

### Supplementary Note 1. Electrical transport properties

Electrical transport properties of Se-doped $Mg_3Sb_{1.5}Bi_{0.5}$ show hysteresis during heating and cooling. Despite of the thermal hysteresis, the hysteresis loop of the resistivity is stabilized after the first cycle and consistent upon the repeated heating and cooling measurements for the following 4 cycles (Fig. S1 and S2). In addition, the thermoelectric $zT$ of the high performance pellet $Mg_{3.07}Sb_{1.5}Bi_{0.48}Se_{0.02}$ (Fig. S4), obtained from the 4 stabilized cycles of resistivity data, shows only very minor hysteresis and excellent consistency between different cycles, indicating that the hysteresis does not affect the overall thermoelectric performance. *In situ* PXRD data show there is no structural change for both the top and bottom surface of the pellets for 4 thermal cycles (Fig. 2). The above results thus indicate that the hysteresis is most likely caused by the reversible processes. The changing microstructure with thermal cycles might be the reason of the hysteresis, which will require further analysis from future work.

### Supplementary Note 2. The three band model

Electrical transport properties of n-type $Mg_3Sb_{1.5}Bi_{0.5}$ in the main text are simulated using a three band model, which considers the effect from the accurate conduction band minimum $CB_1$, the secondary conduction band K, and the valence band Γ. Due to nearly the same band topology as $Mg_3Sb_2$, the effective masses of the $CB_1$, K and Γ bands of $Mg_3Sb_2$ from our previous work[3] are adopted in the model. The relative energies between the K and $CB_1$ band as well as the energy gap are taken from the effective band structure of $Mg_3Sb_{1.5}Bi_{0.5}$. The physical parameters used in the model of n-type $Mg_3Sb_{1.5}Bi_{0.5}$ are summarized in Table S3. Most of the parameters are obtained from *ab initio* calculations. In the model, we treat the $CB_1$ and Γ bands as the Kane bands considering the nonparabolicity, whereas the K band is modeled as a parabolic band.

In this work, we consider the combined alloy scattering, acoustic phonon scattering, and polar optical scattering to understand the electrical transport properties in n-type $Mg_3Sb_{1.5}Bi_{0.5}$.

The total carrier's scattering time is calculated by the Matthiessen's rule $\tau^{-1} = \tau_{al}^{-1} + \tau_{po}^{-1} + \tau_{ac}^{-1}$. Under the framework of the Kane band model, the carrier's scattering time for acoustic phonon scattering based on the deformation potential theory[5] can be written as:[6]

$$\tau_{ac} = \frac{\hbar C_l N_V}{\pi k_B T \Xi^2} g(\varepsilon)^{-1} \left[ 1 - \frac{8\beta(\varepsilon + \varepsilon^2\beta)}{3(1+2\varepsilon\beta)^2} \right]^{-1} \quad (1)$$

$$g(\varepsilon) = \frac{2^{1/2} m^{*3/2} (k_B T)^{1/2}}{\pi^2 \hbar^3} (\varepsilon + \varepsilon^2\beta)^{1/2} (1 + 2\varepsilon\beta), \quad (2)$$

where $\hbar$ is the reduced Plank's constant, $T$ is the absolute temperature, $k_B$ is the Boltzmann constant, $m^*=N_v^{2/3} m_s^*$ is the density of states effective mass, $N_v$ is the valley degeneracy of the electronic band, $m_s^*=(m_{kx} m_{ky} m_{kz})^{1/3}$ is the single valley effective mass, $\varepsilon$ is the reduced energy, $\Xi$ is the acoustic deformation potential, $\beta$ is defined as $k_B T/\varepsilon_g$, here $\varepsilon_g$ represents the energy gap at the k point where the specific band minimum occurs. For instance, for $CB_1$, $\varepsilon_g$ means the energy gap between the conduction band and the valence band at $CB_1$. For the K band, $\beta$ = 0 is chosen for the parabolic band approximation. $C_l$ is the average longitudinal elastic constant for muti-valley systems, which can be estimated by[5]

$$C_l = \frac{3}{5} C_{11} + \frac{4}{5} C_{44} + \frac{2}{5} C_{12} \quad (3)$$

where $C_{11}$, $C_{44}$, and $C_{12}$ are the elastic constants. From the reported elastic constants in ref. 4, we can calculate the $C_l$ values for $Mg_3Sb_2$ (45.6 GPa) and $Mg_3Bi_2$ (56.4 GPa), respectively. Assuming a linear relation of $C_l$ with the faction $x$ in $Mg_3Sb_{2-x}Bi_x$, we can estimate $C_l$ = 48.3 GPa for $Mg_3Sb_{1.5}Bi_{0.5}$.

The carrier's scattering time for the alloy scattering can be expressed as:[7]

$$\tau_{al} = \frac{4\sqrt{2}\hbar^4 (\varepsilon + \varepsilon^2\beta)^{-1/2} (1+2\beta\varepsilon)^{-1}}{3\pi\Omega x(1-x) E_{al}^2 m^{*3/2} (k_B T)^{1/2}} \left[ 1 - \frac{8\beta(\varepsilon + \varepsilon^2\beta)}{3(1+2\varepsilon\beta)^2} \right]^{-1}, \quad (4)$$

where $\Omega$ is the volume per atom, $x$ is the factional ratio of the alloy atom, $E_{al}$ is the alloy scattering potential, which is induced by the atomic level disorder in the solid solution. $E_{al}$ in $Mg_3Sb_{1.5}Bi_{0.5}$ is fit to be 1.0 eV.

If the lattice contains more than one species of atoms, the charge carriers might be scattered by the varying dipole moment because of the optical vibration.[8] The carrier's scattering time for the polar optical scattering is given by:[8,9]

$$\tau_{po} = \frac{2^{3/2}\pi\hbar^2 N_V^{1/3}\varepsilon^{1/2}}{(k_B T)^{1/2} e^2 m^{*1/2}(\varepsilon_\infty^{-1} - \varepsilon_0^{-1})}(1+2\beta\varepsilon)^{-1}(1+\beta\varepsilon)^{1/2}\left\{1-\delta\ln(1+\frac{1}{\delta}) - \frac{2\beta\varepsilon(1+\beta\varepsilon)}{(1+2\beta\varepsilon)^2}[1-2\delta+2\delta^2\ln(1+\frac{1}{\delta})]\right\}^{-1}. \quad (5)$$

Here, $\varepsilon_0$ and $\varepsilon_\infty$ represent the static and high-frequency dielectric constants in units of F/m. The dielectric constants of $Mg_3Sb_{1.5}Bi_{0.5}$ were calculated by density functional perturbation theory[10] (DFPT) in VASP code.[11] The energy convergence criterion was set at $10^{-6}$ eV and a gamma-centered k-point mesh 9×9×6 was used. The isotropic average values of the dielectric tensors were then calculated to be $\varepsilon_0 = 17.4$ and $\varepsilon_\infty = 15.7$ (in relative units), which are used in the model of the polar optical scattering. $\delta$, as a function of the reduced energy, is expressed as:[8,9]

$$\delta(\varepsilon) = \frac{N_v^{2/3} e^2 m^{*1/2}(1+\varepsilon\beta)^{-1}}{\sqrt{2}\varepsilon(k_B T)^{1/2}\pi\hbar\varepsilon_\infty}\,{}^0F_1^{1/2}, \quad (6)$$

where the generalized Fermi integral is defined as:

$${}^nF_l^m(\beta,\eta) = \int_0^\infty (-\frac{\partial f_0}{\partial\varepsilon})\varepsilon^n(\varepsilon+\beta\varepsilon^2)^m(1+2\beta\varepsilon)^l d\varepsilon. \quad (7)$$

$\eta = E_F/k_B T$ is the reduced Fermi energy, and the Fermi distribution function is

$$f_0(E) = \frac{1}{\exp(\varepsilon-\eta)+1}. \quad (8)$$

With the total carrier's scattering time calculated by the Matthiessen's rule, we are able to calculate the electrical transport properties:

The chemical carrier concentration:

$$n = \frac{(2m^* k_B T)^{3/2}}{3\pi^2\hbar^3}\int_0^\infty (-\frac{\partial f_0}{\partial\varepsilon})\varepsilon^{3/2}(1+\varepsilon\beta)^{3/2} d\varepsilon \quad (9)$$

Drift mobility:

$$\mu = \frac{e}{m_I^*}\frac{\int_0^\infty (-\frac{\partial f_0}{\partial\varepsilon})\tau(\varepsilon)(\varepsilon+\beta\varepsilon^2)^{3/2}(1+2\beta\varepsilon)^{-1} d\varepsilon}{\int_0^\infty (-\frac{\partial f_0}{\partial\varepsilon})(\varepsilon+\beta\varepsilon^2)^{3/2} d\varepsilon} \quad (10)$$

where the conductivity effective mass $m_I^*$ is estimated by $3(1/m_{kx}+1/m_{ky}+1/m_{kz})^{-1}$.

Electrical conductivity is calculated by $\sigma = ne\mu$

Seebeck coefficient:

$$\alpha = \frac{k_B}{e}\left(\frac{\int_0^\infty (-\frac{\partial f_0}{\partial \varepsilon})\tau(\varepsilon)\varepsilon^{5/2}(1+\beta\varepsilon)^{3/2}(1+2\beta\varepsilon)^{-1}d\varepsilon}{\int_0^\infty (-\frac{\partial f_0}{\partial \varepsilon})\tau(\varepsilon)\varepsilon^{3/2}(1+\beta\varepsilon)^{3/2}(1+2\beta\varepsilon)^{-1}d\varepsilon} - \eta\right) \quad (11)$$

Lorenz number:

$$L = \left(\frac{k_B}{e}\right)^2 \left[\frac{\int_0^\infty (-\frac{\partial f_0}{\partial \varepsilon})\tau(\varepsilon)\varepsilon^{7/2}(1+\beta\varepsilon)^{3/2}(1+2\beta\varepsilon)^{-1}d\varepsilon}{\int_0^\infty (-\frac{\partial f_0}{\partial \varepsilon})\tau(\varepsilon)\varepsilon^{3/2}(1+\beta\varepsilon)^{3/2}(1+2\beta\varepsilon)^{-1}d\varepsilon} - \left(\frac{\int_0^\infty (-\frac{\partial f_0}{\partial \varepsilon})\tau(\varepsilon)\varepsilon^{5/2}(1+\beta\varepsilon)^{3/2}(1+2\beta\varepsilon)^{-1}d\varepsilon}{\int_0^\infty (-\frac{\partial f_0}{\partial \varepsilon})\tau(\varepsilon)\varepsilon^{3/2}(1+\beta\varepsilon)^{3/2}(1+2\beta\varepsilon)^{-1}d\varepsilon}\right)^2\right] \quad (12)$$

The Hall factor:[12] ( $n_H = n / r_H = 1/eR_H$ )

$$r_H = \frac{3K(K+2)}{(2K+1)^2}\frac{\int_0^\infty (-\frac{\partial f_0}{\partial \varepsilon})\tau(\varepsilon)\varepsilon^{3/2}(1+\beta\varepsilon)^{3/2}(1+2\beta\varepsilon)^{-2}d\varepsilon \int_0^\infty (-\frac{\partial f_0}{\partial \varepsilon})\tau(\varepsilon)\varepsilon^{3/2}(1+\beta\varepsilon)^{3/2}d\varepsilon}{\left(\int_0^\infty (-\frac{\partial f_0}{\partial \varepsilon})\tau(\varepsilon)\varepsilon^{3/2}(1+\beta\varepsilon)^{3/2}(1+2\beta\varepsilon)^{-1}d\varepsilon\right)^2} \quad (13)$$

Here *K* is the anisotropy factor of the carrier pocket. The shapes of the Fermi surfaces for the K, $CB_1$, and Γ bands are all ellipsoidal-like. *K* is thus estimated by $m_{kz}/(m_{kx}m_{ky})^{1/2}$. To better describe the non-ellipsoidal feature of the carrier pockets, *K* can also be calculated by $(m_s^*/m_l^*)^{3/2}$.[13] After comparing the above two different definitions, the results of transport properties are nearly the same. Therefore, here we just use the first definition.

Assuming that the reduced Fermi level for the $CB_1$ band is $\eta$, the reduced Fermi levels for the K and Γ bands are then represented by $\eta - \Delta E_{\text{K-CB}_1}$ and $-\eta - E_g$. Using the relations of the reduced Fermi levels, we are able to calculate the electrical transport properties for every individual band. According to the charge neutrality, the total chemical carrier density can be estimated by $n_{total} = n_{CB_1} + n_K - p_\Gamma$. Based on the multiband model proposed by Putley,[14] the total electrical transport properties under the three band model can be simulated by the conductivity-weighted averages:[14]

The total Seebeck coefficient:

$$\alpha_{total} = \frac{\alpha_{CB_1}\sigma_{CB_1} + \alpha_K\sigma_K + \alpha_\Gamma\sigma_\Gamma}{\sigma_{CB_1} + \sigma_K + \sigma_\Gamma} \quad (14)$$

The total electrical conductivity:

$$\sigma_{total} = \sigma_{CB_1} + \sigma_K + \sigma_\Gamma \quad (15)$$

The total Lorenz number:

$$L_{total} = \frac{L_{CB_1}\sigma_{CB_1} + L_K\sigma_K + L_\Gamma\sigma_\Gamma}{\sigma_{CB_1} + \sigma_K + \sigma_\Gamma} \tag{16}$$

The total Hall coefficient:

$$R_H^{total} = \frac{\sigma_{CB_1}^2 R_H^{CB_1} + \sigma_K^2 R_H^K + \sigma_\Gamma^2 R_H^\Gamma}{(\sigma_{CB_1} + \sigma_K + \sigma_\Gamma)^2} \tag{17}$$

The total Hall carrier concentration:

$$n_H^{total} = \frac{1}{eR_H^{total}} \tag{18}$$

The total Hall mobility:

$$\mu_H^{total} = R_H^{total}\sigma_{total} \tag{19}$$

The bipolar thermal conductivity:

$$\kappa_{bip} = T\left[(\alpha_{CB_1}^2\sigma_{CB_1} + \alpha_K^2\sigma_K + \alpha_\Gamma^2\sigma_\Gamma) - \frac{(\alpha_{CB_1}\sigma_{CB_1} + \alpha_K\sigma_K + \alpha_\Gamma\sigma_\Gamma)^2}{\sigma_{CB_1} + \sigma_K + \sigma_\Gamma}\right] \tag{20}$$

Here, the subscripts or superscripts $CB_1$, K, and Γ in the above equations represent the contributions from the conduction bands $CB_1$, K, and the valence band Γ, respectively.

The deformation potential Ξ is a complex parameter, defined as a combination of two deformation components, i.e., $\Xi_d$ and $\Xi_u$, which represent the energy shifts due to the different strain components.[5] For simplicity, here we estimate the relative energy shifts of the $CB_1$, K, and Γ bands from the band structure calculations by mBJ potential[1] in VASP code.[11] The energy shifts of the $CB_1$, K, and Γ bands, with respect to a small uniaxial strain along the a, b, c directions, were calculated by aligning the deep core levels. The applied small strain was ±2%. The average energy shifts of the three principle axes for the $CB_1$, K, and Γ bands are labelled as $\Delta E_{CB_1}$, $\Delta E_K$, and $\Delta E_\Gamma$. The relative ratios of the deformation potentials for the three bands are estimated to be $\Xi_{CB_1} / \Xi_K = \Delta E_{CB_1} / \Delta E_K = 1.7$ and $\Xi_\Gamma / \Xi_K = \Delta E_\Gamma / \Delta E_K = 2.0$. Then, the deformation potentials of the $CB_1$, K, and Γ bands can be represented by $1.7\Xi_K$, $\Xi_K$, and $2.0\Xi_K$. By fitting the experimental Hall mobility versus Hall carrier concentration at room temperature, we get $\Xi_K$ = 13.6 eV and thereby $\Xi_{CB_1} = 23.2$ eV and $\Xi_\Gamma = 27.2$ eV. The deformation potential values were chosen to provide the acceptable fits to the properties and

thereby the fit might not be unique. In this work, the band structure of $Mg_3Sb_{1.5}Bi_{0.5}$ is assumed to be rigid and independent of temperature.

## Supplementary References


(1) Tran, F.; Blaha, P. Accurate band gaps of semiconductors and insulators with a semilocal exchange-correlation potential. *Phys. Rev. Lett.* **2009**, *102*, 226401.

(2) Perdew, J. P.; Burke, K.; Ernzerhof, M. Generalized gradient approximation made simple. *Phys. Rev. Lett.* **1996**, *77*, 3865-3868.

(3) Zhang, J.; Song, L.; Pedersen, S. H.; Yin, H.; Hung, L. T.; Iversen, B. B. Discovery of high-performance low-cost n-type $Mg_3Sb_2$-based thermoelectric materials with multi-valley conduction bands. *Nat. Commun.* **2017**, *8*, 13901.

(4) Zhou, D. W.; Liu, J. S.; Xu, S. H.; Peng, P. Thermal stability and elastic properties of $Mg_3Sb_2$ and $Mg_3Bi_2$ phases from first-principles calculations. *Physica B* **2010**, *405*, 2863-2868.

(5) Herring, C.; Vogt, E. Transport and deformation-potential theory for many-valley semiconductors with anisotropic scattering. *Phys. Rev.* **1956**, *101*, 944-961.

(6) Ravich, Y. I.; Efimova, B. A.; Smirnov, I. A. *Semiconducting Lead Chalcogenides*, Plenum Press, 1970.

(7) Harrison, J. W.; Hauser, J. R. Alloy scattering in ternary III-V compounds. *Phys. Rev. B* **1976**, *13*, 5347-5350.

(8) Ravich, Y. I.; Efimova, B. A.; Tamarchenko, V. I. Scattering of current carriers and transport phenomena in lead chalcogenides II. experiment. *Phys. Status Solidi B* **1971**, *43*, 453-469.

(9) Wang, H.; Schechtel, E.; Pei, Y.; Snyder, G. J. High thermoelectric efficiency of n-type PbS. *Adv. Energy Mater.* **2013**, *3*, 488-495.

(10) Gajdoš, M.; Hummer, K.; Kresse, G.; Furthmüller, J.; Bechstedt, F. Linear optical properties in the projector-augmented wave methodology. *Phys. Rev. B* **2006**, *73*, 045112.

(11) Kresse, G.; Furthmüller, J. Efficient iterative schemes for ab initio total-energy calculations using a plane-wave basis set. *Phys. Rev. B* **1996**, *54*, 11169-11186.

(12) Xie, H.; Wang, H.; Pei, Y.; Fu, C.; Liu, X.; Snyder, G. J.; Zhao, X.; Zhu, T. Beneficial contribution of alloy disorder to electron and phonon transport in half-heusler thermoelectric materials. *Adv. Funct. Mater.* **2013**, *23*, 5123-5130.

(13) Gibbs, Z. M.; Ricci, F.; Li, G.; Zhu, H.; Persson, K.; Ceder, G.; Hautier, G.; Jain, A.; Snyder, G. J. Effective mass and Fermi surface complexity factor from ab initio band structure calculations. *npj Comput. Mater.* **2017**, *3*, 8.

(14) Putley, E. H. Galvano- and thermo-magnetic coefficients for a multi-band conductor. *J. Phys. C: Solid State Phys.* **1975**, *8*, 1837-1840.